

Rainfall-induced landslides in the residual soil of andesitic terrain, western Japan

Ranjan Kumar Dahal. Shuichi Hasegawa. Minoru Yamanaka. Netra Prakash Bhandary, Ryuichi Yatabe

R. K. Dahal

Department of Geology, Tri-Chandra Multiple Campus, Tribhuvan University, Ghantaghar, Kathmandu, Nepal

S. Hasegawa. M. Yamanaka.

Dept. of Safety Systems Construction Engineering, Faculty of Engineering, Kagawa University, 2217-20, Hayashi-cho, Takamatsu City, 761-0396, Japan

N. P. Bhandary, R. Yatabe

Department of Civil and Environmental Engineering, Ehime University, Bunkyo-3, Matsuyama 790-8577, Japan

Phone: 00977-1-4112090

Fax: 00977-14112127

Email: ranjan@ranjan.net.np

Cite this article as: Dahal R.K., Hasegawa S., Yamanaka M., Bhandary N.P., Yatabe R., 2011, *Rainfall-induced landslides in the residual soil of andesitic terrain, western Japan, Journal of Nepal Geological Society*, 42: 127–142.

Abstract

Rainfall triggered landslides are frequent problems in the residual soil of andesitic terrain in west Japan. Characteristics of residual soils over bronzite andesite, procedure of in situ permeability measurement, matric suction and soil moisture content change and stability analyses considering unsaturated-saturated soils as integral system are presented in this paper. The paper highlights two landslides of small andesitic hillock of western Japan and describes modelling of rainwater seepage, slope stability analysis and contributing parameters for landsliding in andesitic terrain. For both landslides, results of geomorphological and geotechnical analyses were used as a direct input to the numerical modelling. For transient conditions, a finite element analysis was used to model the fluctuations in pore water pressure during the rainfall, with the computed hourly rainfall rate as the surface boundary condition. This was then followed by the slope stability analysis using the temporal pore water pressure distributions derived from the seepage analysis. Obtained trend for the factor of safety was indicates that the most critical time step for failure was a few hours following the antecedent moisture content of previously day peak rainfall. Time of failure estimated by modelling has shown good match with time declared by eyewitnesses.

1 Introduction

Landslide occurrence is generally facilitated by combined effect of intrinsic and extrinsic parameters. A trigger is an extrinsic event such as an intense rainfall event, an earthquake, a volcanic eruption, a storm wave, or rapid stream erosion that causes a near-immediate response in the form of a landslide by rapidly increasing the stresses or strains and reducing the strength of the slope-forming materials (Wieczorek, 1996). Similarly, intrinsic parameters also have vital roles in the landslide occurrence and they include bedrock geology,

50 geomorphology, soil depth, soil type, slope gradient, slope aspect, slope curvature, landuse,
51 elevation, engineering properties of the slope material, land use pattern, drainage patterns and
52 so on. When extrinsic parameter rainfall is concerned, the type of landslide largely depends
53 upon intensity and duration of the rainfall events (Campbell 1975; Caine 1980; Brand et al.
54 1984; Wiczorek 1987; Wilson and Wiczorek, 1995; Crozier 1999; Corominas 2000,
55 Guzzetti et al. 2004; Aleotti 2004; Giannecchini 2006; Dahal and Hasegawa 2008). The
56 existing rainfall-induced landslide studies illustrate the general and numerical relationships
57 between landslides and rainfall in various countries. Studies have showed that rainfall can
58 induce both deep- and shallow-seated landslides, but deep-seated landslides are triggered by
59 rainfall over extended periods with a moderate intensity, while shallow landslides such as soil
60 slips and debris flow are usually triggered by short duration and intense precipitations. Slope
61 material permeability has close link with landslide occurrence (Campbell 1975; Crozier 1999;
62 Guzzetti et al. 2004; Dahal and Hasegawa 2008). Granular slope materials tend to react to
63 short duration extreme rainfall events whereas clayey materials are mainly sensitive to a long
64 duration and rather low rainfall intensity. Studies show that critical quantity of rainfall
65 necessary to produce slope failure depends on vegetation, hydrology and morphology of the
66 slope (Campbell 1975; Brand et al. 1984; Wiczorek 1987; Wilson and Wiczorek, 1995;
67 Corominas 2000,).

68 Varieties of approaches have already been described in literatures and they showed the
69 relationship between rainfall and slope failures in terms of rainfall thresholds, hydrological
70 models, and, coupled with hydrological and stability models (Reid et al. 1988; Dhakal and
71 Sidle 2004; Borga et al. 2002, Rezaur et al. 2002; Rahardjo et al. 2002; Tsaparas et al. 2002;
72 Kim et al. 2004; Rahardjo et al. 2005; Dapporto et al. 2005; Tofani et al. 2006; Dahal et al.
73 2008a). Rainfall and liquefaction of slope materials have also been examined by number of
74 researchers (Anderson and Sitar 1995; Montgomery et al. 1997; Sassa 1998; Dai et al. 1999;
75 Lan et al. 2003; Collins and Znidarcic 2004; Cai and Ugai 2004). Rainfall-induced landslides
76 in coarse grained soils are normally caused by increased pore pressures and seepage forces
77 during periods of intense rainfall whereas in fine grained soil having low infiltration rates do
78 not lead to the development of positive pore pressure and failure occurs due to the decrease in
79 shear strength of soils caused by the loss of matric suction. Many studies also suggest that
80 shallow failures are usually associated with the increased positive pore water pressure whilst
81 loss of negative pore water pressure or matric suction is mainly responsible for deep-seated
82 failure (Anderson and Sitar 1995; Lan et al. 2003; Collins and Znidarcic 2004; Cai and Ugai
83 2004, Dahal et al. 2009). The mobilization of debris flows from slides has also been studied
84 (Ellen and Fleming 1987; Iverson 1997; Iverson et al. 1997; Olivares and Picarelli 2003).
85 These authors showed that liquefaction of slope materials plays a key role in debris-flow
86 initiation.

87 Understanding of the distribution of positive as well as negative pore water pressure is a
88 fundamental of rainfall triggered landslide study (Rahardjo et al. 1995). Usually, hydrological
89 models have been used to simulate saturated and unsaturated flow in slopes. The hydrological
90 models can be linked to slope stability models to obtain accurate simulations of the
91 conceivable stability conditions of slope during rainfall. TOPOMODEL (Beven and Kirkby
92 1979), HYSWASOR (Van Genuchten 1980), Combined Hydrology and, Slope Stability
93 (CHASM) model (Anderson and Lloyd 1991; Collison and Anderson 1996) and GWFLUCT
94 (Terlien 1996) are some examples of such hydrological models. The model described by
95 Iverson (2000) illustrates the infiltration process of rainfall and landslide processes. He
96 showed that the use of pressure head response, topographic data, rainfall intensity and
97 duration, along with infinite-slope failure criteria, helps to predict the timing, depth, and
98 acceleration of rainfall-triggered landslides. The Antecedent Soil Water Status Model

99 (ASWSM) described by Crozier (1999) and Glade et al. (2000) accounts for the draining of
100 early rainfall (total flow out of initial rainfall) and accumulation of late rainfall (infiltration of
101 rain later stage). They provide an equation for estimating the probability of landslide
102 occurrence as a function of daily intensity and previous water accumulation. The GeoStudio
103 (2005) software package is another example of a coupled (SEEP/W and SLOPE/W)
104 hydrological-slope stability modelling software. The coupled SEEP/W–SLOPE/W analyses
105 (Krahn 2004a; Krahn 2004b) have been applied successively to evaluate the dynamic
106 conditions of stability of embankments and slopes (Rinaldi and Casagli 1999, Crosta and Dal
107 Negro 2003; Rinaldi et al. 2004; Collins and Znidarcic 2004; Dapporto et al. 2005). The
108 SEEP/W of GeoStudio software package analyses the seepage problems and adopts an
109 implicit numerical solution to solve Darcy’s equation for saturated and unsaturated flow
110 conditions, describing pore-water pressure and movement patterns within porous materials
111 over space and time. The results obtained from seepage modelling can be directly linked to
112 SLOPE/W. Whereas, SLOPE/W can be used as a limit equilibrium slope stability model.

113 The occurrence of rainfall-induced landslides in both residual (Rahardjo et al. 1995; Rahardjo
114 et al., 2002) and colluvial soil (Rinaldi et al. 2004; Dapporto et al. 2005) slopes are common
115 in many tropical and subtropical regions with abundant rainfalls. Rainfall-induced slope
116 failure involves infiltration through the unsaturated zone above the ground water table.
117 Therefore, unsaturated and saturated soils conditions in a slope have to be considered in the
118 stability analyses. Wide ranges of contributing parameters are involved in rainfall-induced
119 landsliding process. Slope geomorphology, micro climate, bedrock structures, bedrock
120 hydrology, saturated and unsaturated strength of the slope materials, clay mineralogy of slope
121 materials, transient pore water pressure changes, and abrupt loss of strength are the main
122 factors found to be responsible for rainfall-triggered landsliding processes (Rahardjo et al.,
123 2002; Rinaldi et al. 2004; Dapporto et al. 2005; Dahal et al. 2009) . In this context, this paper
124 describes a rainfall triggered landsliding process in residual soil of andesitic terrain in
125 western Japan.

126 **2 Research objectives**

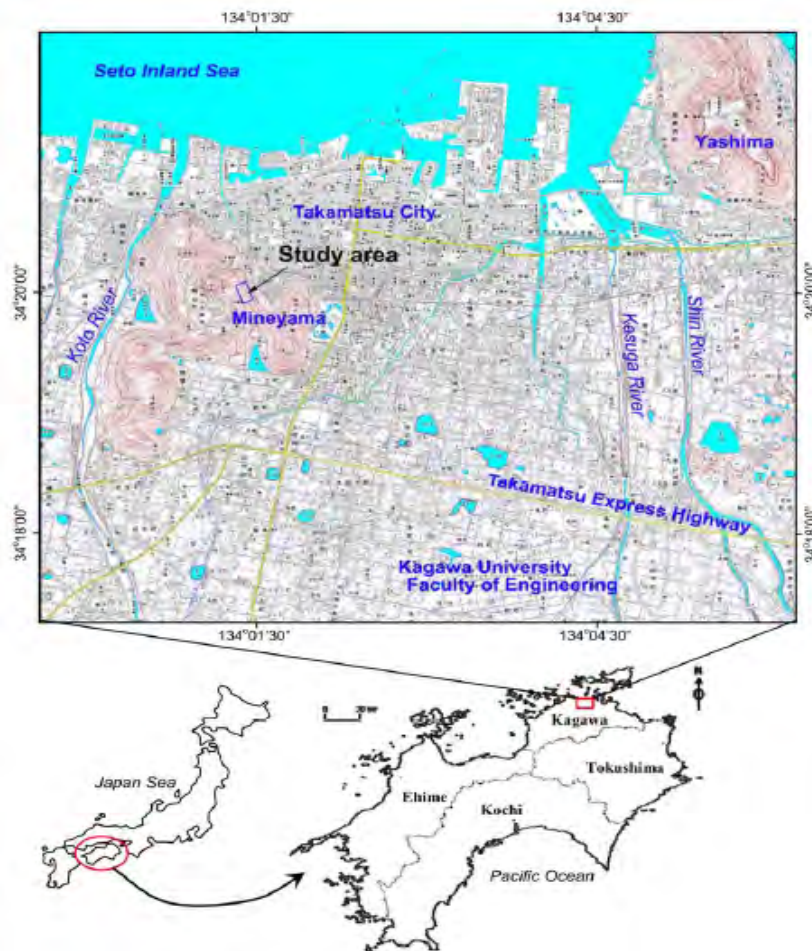
127 The main objective of this study is to investigate the hydro-mechanical process responsible
128 for rainfall-triggered landsliding in residual soils of andesitic terrain of western Japan. For
129 this purpose, a rainfall-triggered landslide event which occurred during an extreme typhoon
130 rainfall of August 2004, in the north eastern hills of Shikoku Island of Japan was selected for
131 the study. Although hundreds of landslides were triggered in both andesitic and granitic
132 terrains (Dahal et al. 2006; Dahal et al. 2008a) in the north-eastern part of Shikoku Island
133 during various typhoons of 2004, the most affected area of andesitic terrain was chosen for
134 the study. Objectives of this research are explicitly listed as follows:

- 135 • To explore the roles of geology and geomorphology setting on the landslide
- 136 • To understand the matric suction change in residual soil of andesitic terrain during
137 different intensity of rainfall
- 138 • To discover the spatial variation of seepage in relation to soil permeability and other
139 physical properties
- 140 • To analyze the stability of slope with respect to high intensity of rainfall and change
141 in pore water pressure
- 142 • To outline the contributing parameters responding for landslide in the andesitic terrain.

143 **3 The study area**

144 **3.1.1 Location and geology**

145 The study area is located in the Mineyama hillock of Takamatsu City of Japan (Fig. 1).
146 Takamatsu, the capital city of Kagawa Prefecture, Japan, is a harbour city on the northern
147 shore of Shikoku Island, Japan. It is the regional administration centre of Shikoku.

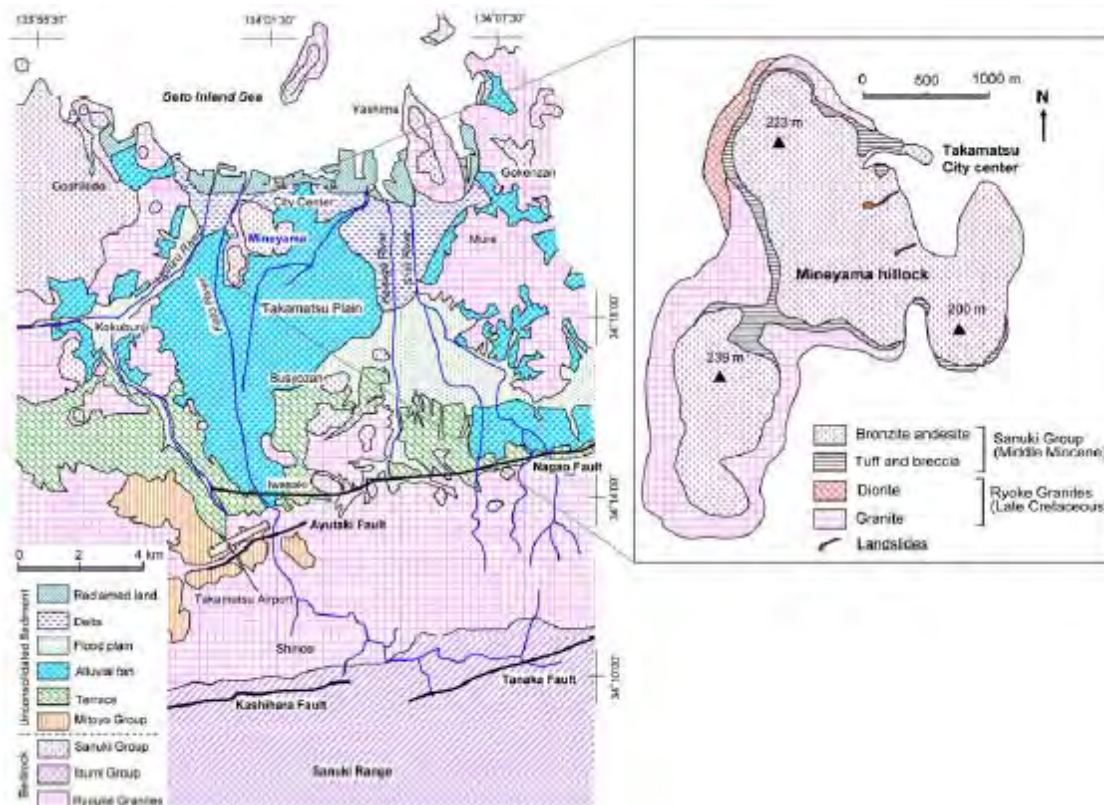


148 **Fig. 1: Location map of study area**

151 Takamatsu City is situated in the Takamatsu plain. The plain is mainly composed of the
152 alluvial fan of the Koto river and the subordinate flood plains of the Shin and Kasuga rivers.
153 The downtown Takamatsu has a well-forested Mineyama hillock in west. The maximum
154 altitude of the Mineyama hillock is 208 m above the mean sea level. The area mainly consists
155 of evergreen broad leaf and deciduous broad leaf types of forest. Japanese red pine (*Pinus*
156 *deniflora*), camphor (*Cinamomum camphora*), Japanese oak (*Quercus serrata* and *Quercus*
157 *variabilis*) are main tree species in the Mineyama. Baby rosa (*Rosa multiflora*) and China
158 root (*Smilax china*) are main shrubs in the forest. The toe of the Mineyama hill, is densely
159 populated and formed a part of downtown Takamatsu. Because of the panoramic view of the
160 Seto Inland Sea and Takamatsu City to the north and east, Mineyama hill is a popular hiking
161 spot.

162 Geologically, Shikoku Island is roughly divided into three geological zones. They are Ryoke,
163 Sambagawa-Chichibu and Shimanto belts from north to south, respectively. Topographically,
164 the Ryoke Belt in Shikoku is divided into three zones: Seto Inland Sea, Recent fan and Hills
165 having a maximum altitude of approximately 1000 m. This belt consists of Late Cretaceous
166 granitic rocks, Late Cretaceous sedimentary rocks (Izumi Group) and Miocene volcanic rocks

167 (Sanuki Group). Being the locality of Izumi Group, Mineyama hill also consist of Miocene
 168 andesite and rhyolite (Fig. 2). Kuno (1947) called andesite as bronzite-andesite because of the
 169 presence of higher percentage of bronzite mineral which locally also known as Sanukite. The
 170 toe of the Mineyama hill mainly consists of colluvium soil having weathered angular pebble
 171 of bronzite-andesite. On the upper hill slope, Mineyama has 1 to 3 m thick residual soil over
 172 bronzite-andesite.



173 **Fig. 2: Geological map of Takamatsu City and Mineyama hillock**

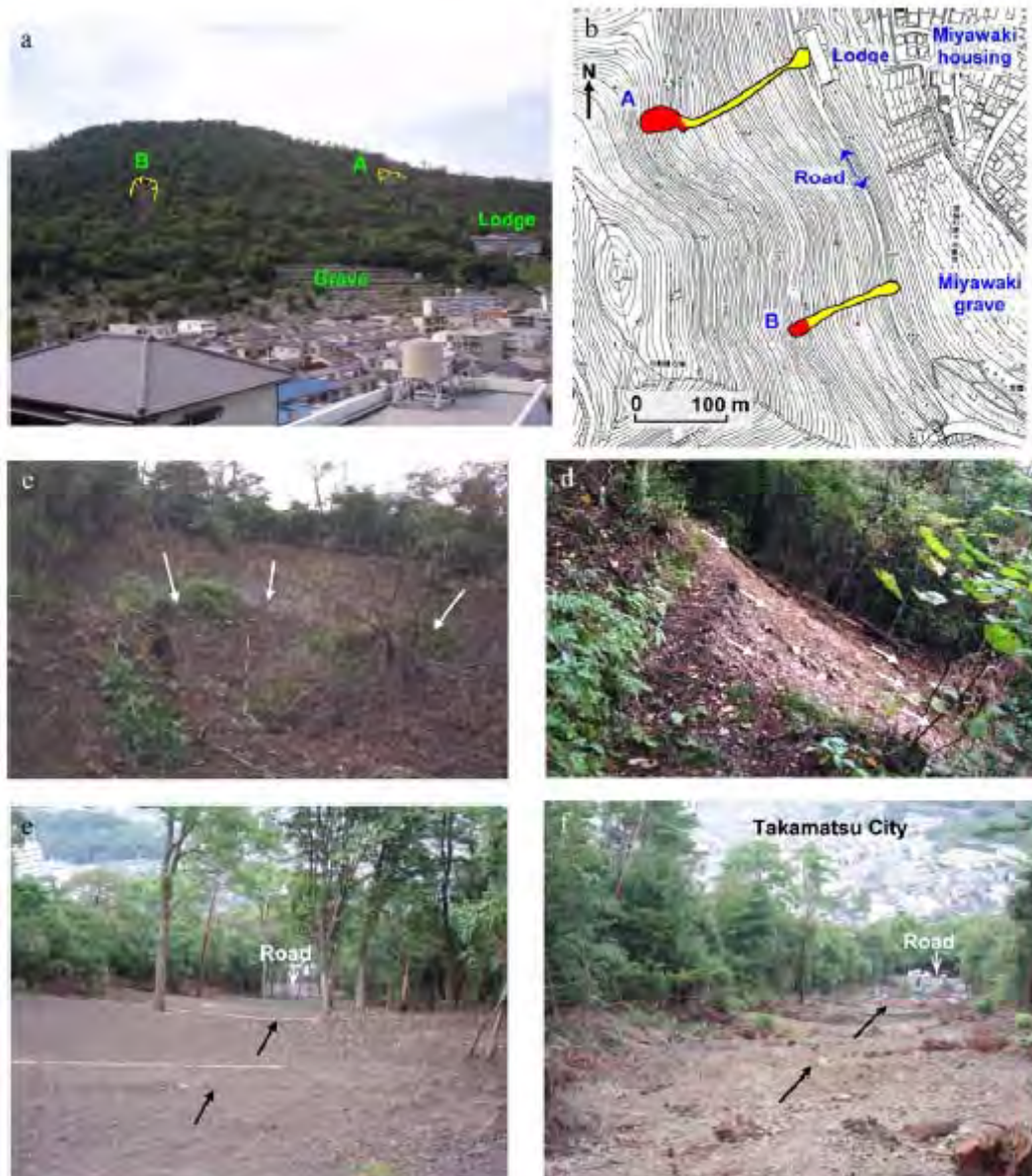
174 **3.1.2 Rainfall and landsliding**

175
 176 Shikoku Island of Japan usually gets extensive typhoon rainfalls in southern part in
 177 comparison to northern part. As a result, rainfall related slope failure phenomena are very
 178 common in central and southern Shikoku. However, northeast Shikoku (Kagawa Prefecture)
 179 is also suffering from some events of slope failures. In the year 2004, all together 10
 180 typhoons hit Japanese archipelago and out of which nine typhoons affected the Shikoku
 181 Island. Storm and flood damages in 2004 resulted in a total of 227 killed and missing in
 182 whole Japan, which is the highest number since 1984 (MLIT, 2004). In 2004, Ehime, Kochi
 183 and Kagawa prefectures were mostly affected by Typhoon 23 and typhoon 21 whereas
 184 typhoons 4, 6, 10, 11, 15, 16 and 18 caused extensive damage and loss of lives in Kochi,
 185 Tokushima and Ehime prefectures (Hiura et al. 2005; Dahal et al., 2008b).

186 In 2004, Kagawa Prefecture badly suffered loss of lives and property due to landsliding
 187 triggered by typhoon rainfall. Better to say, Kagawa was the most affected prefecture. It was
 188 noticed that hourly rainfalls exceeding 50 mm and total 24-hour rainfalls over 200 mm were
 189 the main cause of slope failures at different locations in Kagawa. The hardest-hit areas were
 190 in granitic terrain of eastern Kagawa, granitic, rhyolitic and andesitic terrain around
 191 Takamatsu City (central Kagawa) and sedimentary terrain of western Kagawa (Dahal et al.
 192 2006, 2008b).

193 Two landslides occurred in eastern face of Mineyama hillock during heavy rainfall of 19th
 194 and 20th October of 2004 (Typhoon 0423). A total of 11 landslides occurred in Mineyama
 195 after extreme rainfall owing to typhoon 0416 and 0423. In this study, landslide ‘A’ and

196 landslide 'B' were selected for detailed study (Fig. 3). Landslide 'A' is located at topographic
 197 hollow of uphill section of Mineyama hiking road and front side of Ritsurin lodge. According
 198 to an eyewitness account, landslide 'A' occurred at 14:00 hours of 20th October, 2004. The
 199 debris from the failure accumulated on parking area of a resort and damaged some vehicles.
 200 Landslide 'B' was located on same east facing slope but situated approximately 250 m south
 201 of Landslide 'A' and it is also situated at topographic hollow of uphill section of Mineyama
 202 hiking road. The exact failure time of Landslide 'B' can not be confirmed but it is assumed
 203 that it also failed around the same time as of Landslide 'A'. In both the landslides, failure was
 204 first initiated as debris slide and then started to flow down as debris flow. Hereafter landslides
 205 'A' and 'B' are addressed as Mineyama landslides.



206
 207 **Fig. 3: View of Mineyama landslides. a. Photographic view of landslides 'A' and 'B', b.**
 208 **Topographical settings of Mineyama landslides, c. Scar of landslide 'A' after failure, d.**
 209 **Scar of landslide 'B' immediately after failure, e. Down slope view of landslides 'A' in**
 210 **October 2005 and f. Downslope view of landslides 'B' in October 2005**
 211

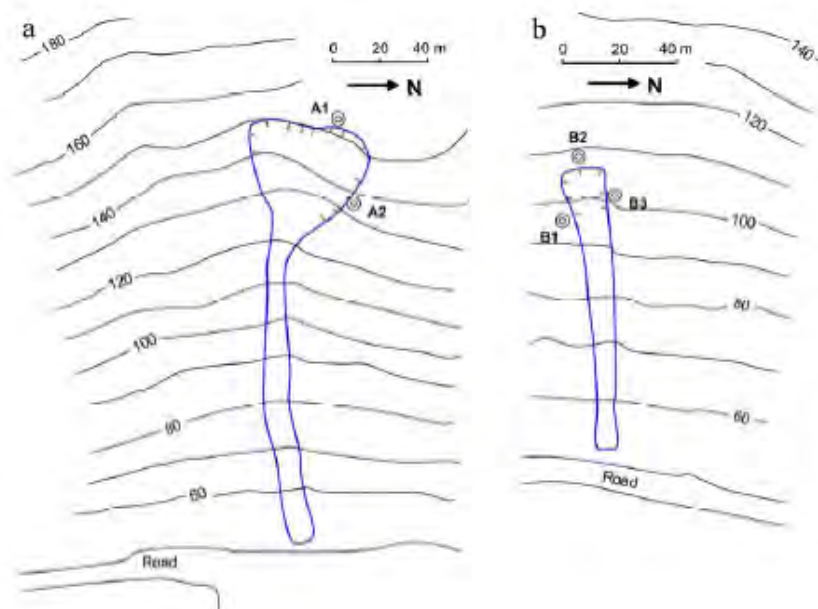
212 **4 Methodology**

213 **4.1.1 Field Investigations**

214 A total of 22 days of field visits and observations as well as measurements were carried out in
215 the Mineyama landslides site in the year 2004, 2005, 2006 and 2007. The first preliminary
216 field observations in the study area were performed immediately after the main landslide
217 events in 2004. The regular visits has been made in 2005, 2006, and 2007 to observe the
218 change in vegetation and response of the slopes during various rainfall events in these years.
219 In the typhoon season of 2007, a detailed field investigation of permeability and matric
220 suction test was carried out. Soil thickness along the landslide scar and debris flow path was
221 recorded during the field survey. GPS (Global Positioning System) was used to locate
222 landslide scarp.

223 The main factor triggering the Mineyama landslides was extreme rainfall due to typhoon
224 0423 (October 19 and 20, 2004). Thus, permeability of the soil has to be ascertained to
225 understand the hydrological characteristics of the slope materials. Thus, in situ permeability
226 tests were performed. A total of five locations were selected for the permeability tests. The
227 locations of the permeability tests are given in Fig 4., (A1 and A2 at landslide ‘A’ and B1, B2
228 and B3 at landslide ‘B’). These locations were chosen considering the fact that the soil
229 properties on the crown part are responsible for the failure. The locations immediately after
230 the failure scarp were selected for the study.

231 Hasegawa in situ permeability tester was used to determine saturated permeability of soil
232 (Daitou Techno Green, 2009). Tensiometers were used to measure soil matric suction. Soil
233 samples were collected for soil classification, clay mineral identification, and measurement of
234 shear strength parameters in the laboratory. 100 cc tubes were used to collect samples to
235 determine soil density. Undisturbed sample were recovered at locations A1 and B2. However,
236 in other locations, undisturbed sampling was not possible owing to the presence of granule
237 and small pebble in soil. So, disturbed samples were taken from those locations.



238 **Fig. 4: Location of in situ permeability test, a. in landslide ‘A’ and b. in landslide ‘B’**

240 **4.1.2 Hasegawa in situ permeability tester**

241 Hasegawa in situ permeability tester kit is a simple and easy to use in situ soil permeability
242 test kit developed by Daitou Techno Green, Inc., Japan. Basically, till date, it has been used
243 to understand ground permeability for tree and shrub plantation. In this research, Hasegawa

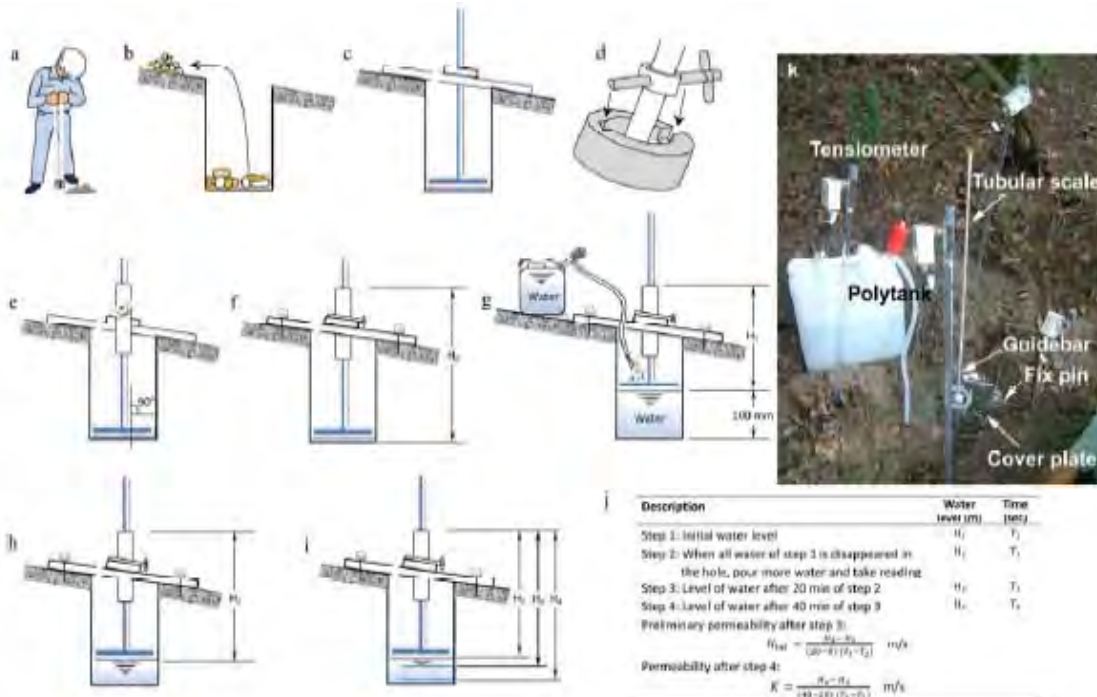
244 in situ permeability tester was used for landslide study. Total five permeability tests were
245 performed at locations A1, A2, B1, B2, and B3.

246 The Hasegawa permeability test kit consists of hole cover plate, float plate, scale of 60 cm
247 and 100 cm, fixed pin and scale guide are main parts of the test kit. Each set of test kit is
248 provided with double sets of accessories. As a result, simultaneous test on two nearby site are
249 possible in one attempt. Depending upon the slope materials, ten to twenty litres of water is
250 necessary for each test. Poly tank of twenty litres capacity is suitable for this purpose. Brief
251 summary of test procedures are as follow.

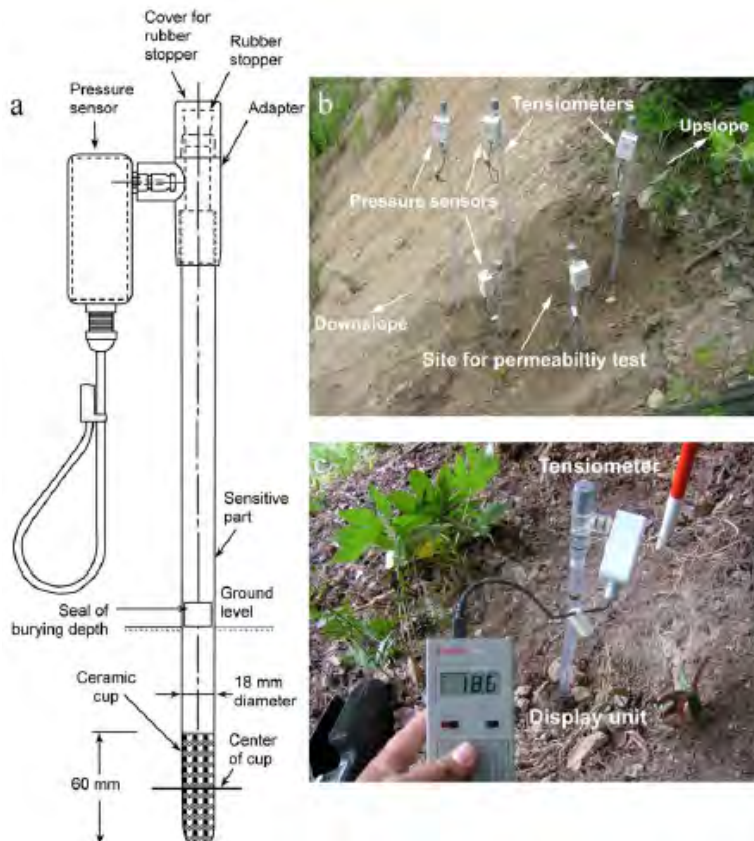
- 252 1. Remove any upper part of organic materials of sites.
- 253 2. Make a hole of 20 to 40 cm deep using double scoop shovel (Fig. 5a).
- 254 3. Remove any gravel materials from base of the hole (Fig. 5b).
- 255 4. Install tubular scale with float plate and insert within scale guide bar (Fig. 5c).
- 256 5. Place hole cover plate, fix it by fix pin and tight scale guide bar with cover plate (Fig.
257 5d and Fig. 5e).
- 258 6. Note down reading of tubular scale when float attached with tubular scale touch base
259 of hole (Fig. 5f).
- 260 7. Use siphon to pour water from poly tank into the hole (Fig. 5g).
- 261 8. Fill test hole with water and wait for one hour.
- 262 9. After one hour, again fill test hole with water and take reading of tubular scale after
263 20 minutes and 40 minutes (Fig 5h.).
- 264 10. If water is finished before 20 or 40 minutes, note down that time (Fig 5i.).
- 265 11. Relationship given in Fig 5j. is used to determine permeability of the soil layer in m/s.

266 **4.1.3 In situ soil matric suction test**

267 Commercially available Daiki tensiometer was used to measure in situ soil matric suction For
268 the measurement of soil matric suction, display type tensiometer having ceramic sensitive
269 part and pressure sensor was used in field. Illustration of Daiki tensiometer with display unit
270 is given in Fig. 6. Twenty three locations were selected for soil matric suction of which eight
271 locations were selected at Landslide 'A' and 15 locations were selected at Landslide 'B'.
272 Matric suction test points were located on both left and right as well as up slope and down
273 slope of permeability test location as shown in Fig. 6. To get the best results and to allow
274 good contact between soil and ceramic cup, tensiometers was installed 24 hours before the
275 data measurement. Data were taken from all tensiometers to understand the spatial variation
276 of soil matric suction around permeability test site.



277
 278 **Fig. 5: Schematic illustrations of the Hasegawa in situ permeability tester and**
 279 **permeability determination method. ‘a’ and ‘b’ demonstrate process of excavation of**
 280 **hole and removing of any coarse materials on the base. Installation of tubular scale**
 281 **with float plate is illustrated in ‘c’, ‘d’ and ‘e’. ‘g’, ‘h’ and ‘i’ demonstrate data**
 282 **measurement procedure. Short description of procedure and method of calculation of**
 283 **permeability is shown in ‘j’. Permeability test at location B3 is shown in ‘k’.**
 284 During the permeability test, data of matric suction were also taken at 5 min interval to get
 285 the information on the changes in matric suction during water percolation. However,
 286 noticeable changes in matric suction were not evident throughout the permeability test period
 287 since the soil permeability was relatively low.



288
289 **Fig. 6: a. Schematic drawing of tensiometer, b. Installation of tensiometers in location**
290 **A4 (scar of landslide 'A'), c. Display unit and matric suction reading at location B2.**
291

292 **4.1.4 Vegetation and root study**

293 The role played by vegetation in improving slope stability is well recognized and
294 comprehensive reviews are found in the literature (Gray et al. 1980; Greenway 1987; Morgan
295 and Rickson 1995; Howell 1999a and 1999b; Schmidt et al. 2001). Vegetation enhances
296 slope stability via root reinforcement. Therefore, root reinforcement is also considered in this
297 study because penetrating vertical taproots and sinker roots provide additional stability to the
298 slopes.

299 A certain amount of research has been done on the forested hill slopes (Wu et al. 1979; Sidle
300 1991; Kondo et al. 2004; Nghiem et al. 2004; Kubota et al. 2004) to understand hill slope
301 stability and root cohesion. Kubota et al. (2004) has mentioned that slope having deciduous
302 broad leaves and mixed forest can have effective cohesion value in between 4.9 kN/m² and
303 6.8 kN/m². Kondo et al. (2004) has developed equations to estimate root cohesion with the
304 help of root diameter and tensile strength.

305 The root shear resistance force (S_r) can be expressed on the basis of equilibrium of acting
306 force (Waldron 1977, Wu et al. 1979, Kondo et al. 2004) as follow. Detail calculations is
307 available in Kondo et al. 2004 and Fig. 7 was used for parameter illustration.

308
$$S_r = t(\sin \theta_r + \cos \theta_r \tan \phi) \dots \dots \dots (1)$$

309 Where, θ_r is inclination angle and ϕ is internal friction angle.

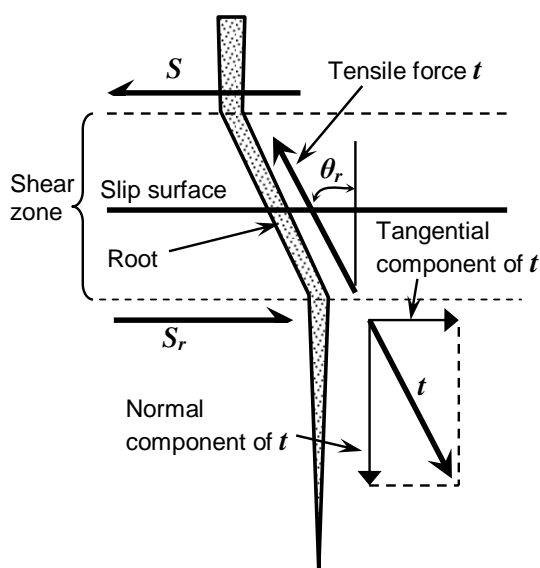
310 Eq. 1 suggests that if internal friction angle is given, the root shear-resistance (S_r) can be
311 derived with the value of tensile strength and inclination angle (θ_r) of root. Hayashi (1998)
312 has proposed the relationship of tensile strength (t) and the diameter (d) of root at the
313 breaking point with a regression equation as follow.

314
$$t = k_p d^{2.03} \dots \dots \dots (2)$$

315 Where k_b is a correlation coefficient and its value is used according to plant species (Kondo et al. 2004).
 316 Wu et al. (1979) has proposed that the angle of θ_r usually range in between 48
 317 degrees to 72 degrees. Thus, for n roots of per square meter, root cohesion c_r can be
 318 expressed as follow (Kondo et al. 2004).

319
$$c_r = \sum_{i=1}^n S_{ri} \dots\dots\dots (3)$$

320 From Eq. 3, vegetation root characteristics at landslide scar were recorded in the field. The
 321 number of roots per sq. m in the landslide scarp were counted. A total of five locations were
 322 selected for the root density measurement. In each location, diameter of plant root at landslide
 323 scarp was noted. A total of 40 records of root diameters were measured from five locations in
 324 both landslides ‘A’ and ‘B’ and used to calculate root tensile strength as per the Eq. 2.
 325 Minimum value of θ_r , described by Wu et al. (1979), were also considered in the calculation
 326 and apparent root cohesion values at locations A and B were determined and used in stability
 327 analysis.



344 **Fig. 7: Reinforcement mechanism in soil with root (modified after Kondo et al. 2004)**

345 **4.1.5 Experimental investigations**

346 Soil samples collected from all five locations in both landslides ‘A’ and ‘B’ were investigated
 347 in the laboratory for index property identification, clay mineralogy, and shear strength
 348 parameter. All index parameters were determined in the laboratory along with the grain size
 349 distribution. Direct shear tests were conducted in undisturbed as well as reconstituted soil
 350 specimens. The soil sample was reconstituted with sieved material finer than 2 mm to
 351 eliminate large fragments that could have altered the measurements. All tests were performed
 352 in saturated and drained conditions. The applied normal pressure ranged between 100 and
 353 300 kN/m². X-ray diffraction analysis was employed to identify the constituent clay minerals
 354 in the soil. The powder method was used for the X-ray diffraction analysis, in which all
 355 particles were crushed into fine powder and constituent minerals were identified using X-ray
 356 diffraction patterns. The ethylene glycol treatment method was used to confirm the expansive
 357 minerals of low values of 2θ (less than 15° , θ is angle of incidence of x-ray).

358 **4.1.6 Hydrological and stability analysis**

359 Hydrological and stability analysis were performed to analyse the variation of pore water
 360 pressure and slope instability in the Mineyama landslides. The modelling of transient pore
 361 water pressure and slope stability has done with finite element method (FEM) based

362 computer applications namely SEEP/W and SLOPE/W (GeoStudio, 2005). Modelling
 363 parameters has obtained from both field and laboratory investigations as well as from the
 364 literatures. In SEEP/W and SLOPE/W, the model code is based upon the equations of motion
 365 and mass conservation. Both saturated and unsaturated flows in soil were simulated using a
 366 modified version of Darcy's law. For unsaturated soil conditions, the hydraulic conductivity
 367 function of a soil is described by the relationship between water content and pore water
 368 pressure (Fredlund and Rahardjo, 1993). In case of transient flow, the hydraulic head is no
 369 longer independent of time and volumetric water content changes with time. Thus, Richard's
 370 equation is suitable for describing transient flow (Richards 1931; Fredlund and Rahardjo
 371 1993) as follows:

$$\frac{\partial}{\partial x} \left(k_x \frac{\partial H}{\partial x} \right) + \frac{\partial}{\partial y} \left(k_y \frac{\partial H}{\partial y} \right) + q = \frac{\partial \theta}{\partial t} \dots\dots\dots(4)$$

372 where H is total head, k_x is hydraulic conductivity in the x-direction, k_y is hydraulic
 373 conductivity in the y-direction, q is applied boundary flux, θ is volumetric water content, and
 374 t is time.
 375

376 The state of stress and soil properties influence the change in the volumetric water content of
 377 soil, and for both saturated and unsaturated conditions, the state of stress is usually described
 378 in the form of $\sigma - u_a$ and $u_a - u_w$ (Fredlund and Morgenstern 1976, 1977; Fredlund and Rahardjo,
 379 1993). The parameter σ is the total stress, u_a is the pore air pressure, and u_w is the pore water
 380 pressure. SEEP/W assumes that the pore air pressure remains constant at atmospheric
 381 pressure during transient flow. Hence, $\sigma - u_a$ does not influence the changes in volumetric
 382 water content; rather, the stress variable $u_a - u_w$ is responsible for changes in volumetric water
 383 content. When considering u_a is considered as a constant variable, the change in volumetric
 384 water content solely depends on the pore water pressure changes. As a result, the change in
 385 volumetric water content can be related to a change in pore water pressure and Eq. 4 can be
 386 written in the form of the soil-water characteristics function (relation between the volumetric
 387 water content and the negative pore water pressures) as follows (Fredlund and Rahardjo,
 388 1993; Tsaparas et al. 2002):

$$\frac{\partial \theta}{\partial t} = m_w^2 \frac{\partial u_w}{\partial t} = m_w^2 \rho_w g \frac{\partial H}{\partial t} \dots\dots\dots(5)$$

389 where m_w^2 is the coefficient of volumetric water change with respect to a change in negative
 390 pore water pressure, i.e. soil matric suction ($u_a - u_w$) and is equal to the slope of the soil water
 391 characteristic curve, ρ_w is the density of water, and g is gravitational acceleration.
 392

393 Combining Eqs. 4 and 5 gives

$$\frac{\partial}{\partial x} \left(k_x \frac{\partial H}{\partial x} \right) + \frac{\partial}{\partial y} \left(k_y \frac{\partial H}{\partial y} \right) + q = m_w^2 \rho_w g \frac{\partial H}{\partial t} \dots\dots\dots(6)$$

394 Eq. 6 is the final form of the governing equation of water flow through the unsaturated soil
 395 and it is an explicitly non-linear equation. SEEP/W uses finite elements to solve Eq. 6. To
 396 obtain the numerical solution of Eq. 6 in SEEP/W, it is necessary to provide the permeability
 397 function (permeability with respect to water versus negative pore water pressure), soil-water
 398 characteristic curve, boundary flux, and initial hydraulic head in the course of defining the
 399 problem.
 400

401 5 Results of investigations

402 5.1.1 Geology and Geomorphology

403 As already discussed under the heading study area, the main rock type in the landslide area is
 404 bronzite-andesite and it is moderately weathered. The rock is dark grey in colour and gives
 405 strong metallic sound when hammer or when two rock pieces struck together. The rocks on
 406 the landslides scar are extensively fractured. Poorly defined sheet joints are also noticed on

407 the scar of landslide A, however, at scar of landslide of B, colluvium soil cover is
 408 predominant.

409 Length of the both landslide slope is less than 200 m and both slides are in similar elevation,
 410 and have the same types of vegetation, rocks, and soils. The upslope is relatively rockier than
 411 the central and lower part of the slope. Geomorphologically, both slides are situated on
 412 topographic hollow or zero-order basin. Slope curvature strongly suggests that the both
 413 landslide scars are situated on the highly susceptible zone of rainwater accumulation.

414 **5.1.2 Geotechnical characterization of soils**

415 The stratigraphy at the selected sites on Mineyama landslides includes homogenous residual
 416 soil and bedrock bronzite andesite. In both Mineyama landslides, failure surfaces were found
 417 at the contact between the residual soil and moderately weathered bedrock. The grain size
 418 distribution curves of the soils are shown in Fig. 8. Unified soil classification of the soil
 419 shows that the soil type of the selected sites is mainly silty clay of medium plasticity with
 420 sand and gravel. The soils from all the five locations have more than 50% fine materials.
 421 Their grain size distribution curves are more or less the same for finer portion. The in situ
 422 permeability tests revealed that Mineyama landslides have permeability in the range of 10^{-7}
 423 m/s to 10^{-8} m/s. The in situ matric suction measurements suggest that increase in rainfall
 424 causes a decrease in soil matric suction. A total five cycles of measurements were taken
 425 between June 26 to July 15, 2007. A maximum soil matric suction of 61.4 kPa and a
 426 minimum 0.6 kPa were measured at different locations of the investigated area during the
 427 period. During one of the investigation periods, typhoon 0704 (named as Man-Yi) hit the
 428 sites and the soil matric suction fluctuations in the soils were recorded. Abrupt change in soil
 429 matric suction and moisture content were observed with frequent rainfall during investigation
 430 period (Fig. 9).

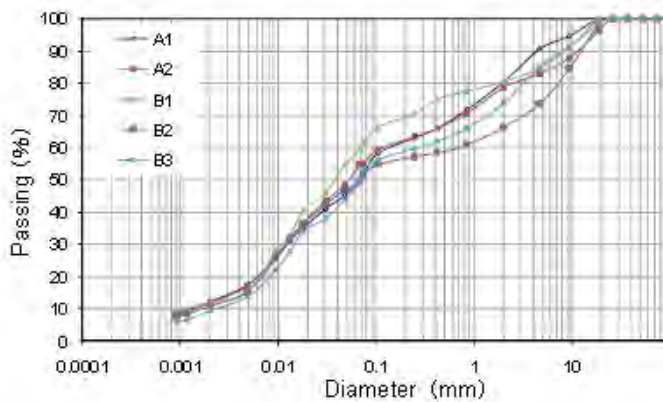
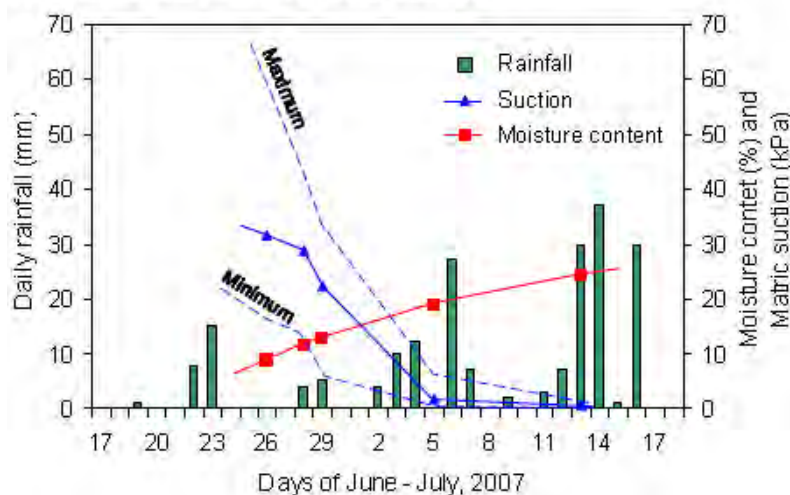


Fig 8, Grain size distribution curve of soils in selected sites



431

432

433 **Fig. 9: Variation of matric suction and moisture content of soils at Mineyama landslides**
 434 **site during typhoon rainfall of 2007. Average matric suction and moisture content are**
 435 **used in this plot. Maximum and minimum value ranges of matric suction are also shown**
 436 **in graph.**

437

438 From Eq. 3, root cohesion of the Mineyama landslides site has also estimated. The soil data
 439 obtained for both the landslides is given in Table 1. The data obtained were used for
 440 hydrological and stability analysis. Cohesion and friction angle were estimated by direct
 441 shear test and root cohesion estimation method (Eq. 3), volumetric water content in saturation
 442 and unit weight were estimated in the lab. Soil permeability was measured in field. These
 443 parameters were used in hydrological and stability analysis.

444 The results of the x-ray diffraction tests are provided in Table 2. From the X-ray diffraction
 445 patterns, it is clear that the main constituent minerals of the samples are quartz, feldspar,
 446 metahalloysite, smectite, and illite.

447 **Table 1. Geotechnical properties of Mineyama landslides (A and B).**

Landslide	Average slope angle (°)	Landslide scarp length (m)	Effective cohesion* (kN/m ²)	Unit weight* (kN/m ³)	Effective friction* angle (°)	Volumetric water content (%)	Hydraulic conductivity (m/s)
A	25.5	46	4.4	13.1	21.5	45	1.167 × 10 ⁻⁷
B	26.5	25	5.2	13.7	19.4	45	1.111 × 10 ⁻⁷

448 *These values are mean values and factor of safety distribution via sensitivity calculation was
 449 performed during stability analysis.

450 **Table 2. Result of X-ray analysis of soils collected from Mineyama landslides site**

Landslide	Quartz	Feldspar	Metahalloysite	Orthopyroxene	Smectite	Illite
A	+++++	++++	++	++	++	+
B	+++++	+++	++	++	+	+
Abundance: ++++++ high + low						

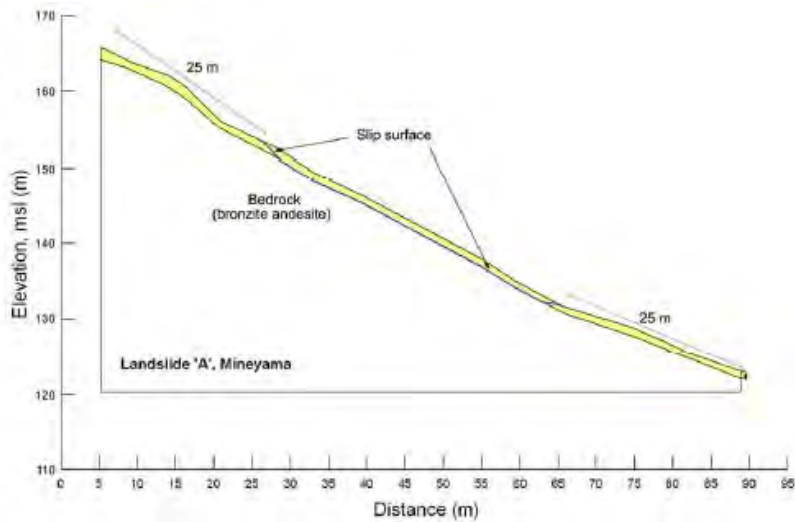
451

452 6 Hydrological and slope stability modelling

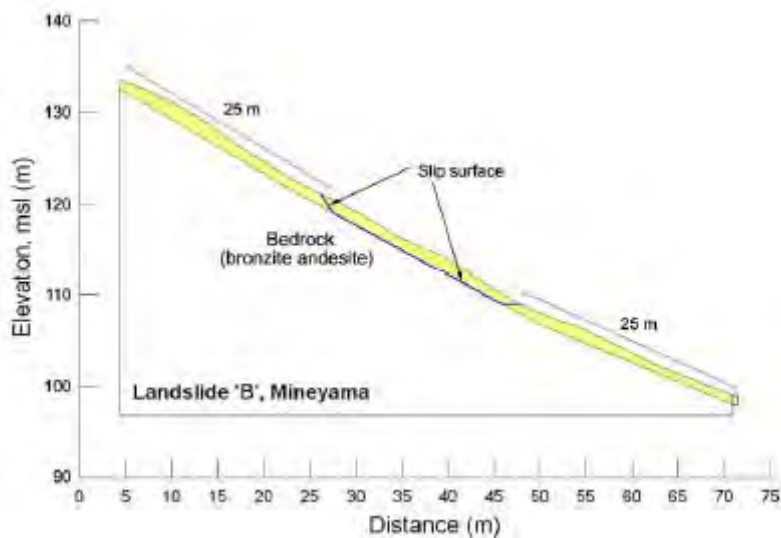
453 6.1.1 Model parameters

454 For the hydrological and slope stability modelling in [GeoStudio \(2005\)](#), both laboratory and
 455 field data were used to assess the hydraulic properties of the residual soils. The thickness of
 456 the residual soil layers were selected as per the field measurements. In Mineyama landslides,
 457 thickness of soil layer range from 0.7 m to 1.8 m. Both landslide affected slopes were
 458 modelled by adopting slope angles measured in the field. Taking reference of the landslides
 459 scarp, 25 m up slope and 25 m down slope length was used in modelling along with total
 460 length of scarp as shown in [Fig. 10](#). Locations of the scarps were fixed from GPS data and
 461 field measurements. Contact between soil and rock was considered to be geometrically planar,
 462 having soil layers parallel to the ground surface. The geotechnical parameters presented in
 463 [Table 1](#) were used in the modelling.

464 The volumetric water content and the hydraulic conductivity functions were obtained from
 465 curves derived using similar grain size distributions function provided in [GeoStudio \(2005\)](#)
 466 by adjusting the saturated water content and permeability values to the actual measured
 467 values. The main failure events occurred on 20th October 2004, and it is difficult to describe
 468 the initial pressure distribution prior to the rainfall events because almost all days of October
 469 have considerable rainfall and no data were available for pore pressure variation. Thus, the
 470 simulation has performed considering typhoon rainfall of 19th and 20th October of 2004.



471



472

473

474

475

476

477

478

479

480

481

482

483

484

485

Fig. 10: Slope geometry of landslide ‘A’ and landslide ‘B’ locations at Mineyama hillock
 Rainfall started at 4:00 hours on the 19th October. The time and the date were set as a start up point, and the initial water table has defined above the bedrock with a maximum negative pore pressure of 61.4 kPa. For the boundary conditions, a transient flux function with values equal to the hourly rainfall intensity for 19th and 20th October of 2004 has applied to the nodes along the ground surface. A null flux condition has assigned to the upslope and down slope vertical faces of the model. In the case of the down slope vertical face, potential seepage face review option and the infinite elements was also selected to extend the actual right edge to infinity in the positive x-direction, to avoid an unnatural impermeable border, and minimize any side effects. Null flux boundary has also imposed at the lower boundary of both simulations. The complete layout of model is shown in Fig. 11. The homogeneous residual soil above the bedrock was considered as single layer for modelling. A null flux condition was assigned to the upslope, down slope and lower boundaries of soil layer.

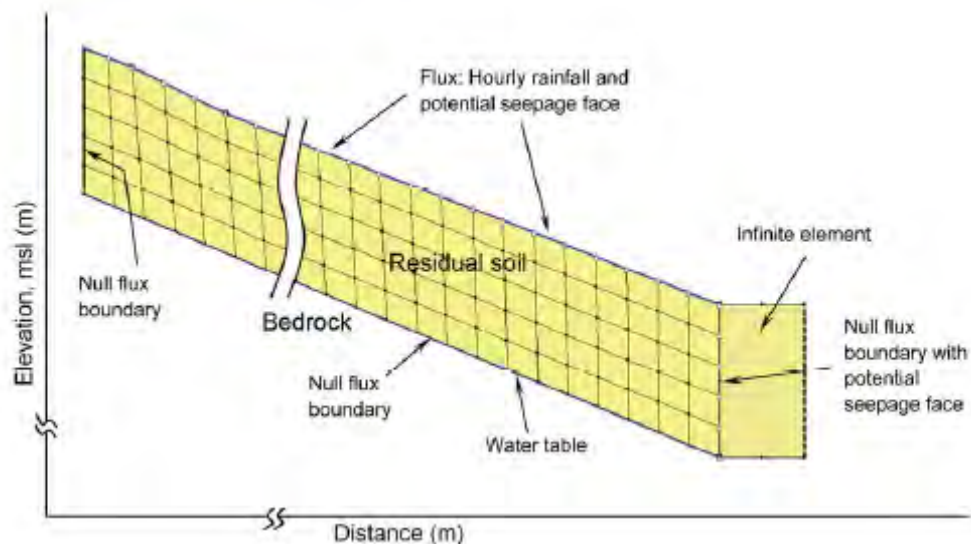


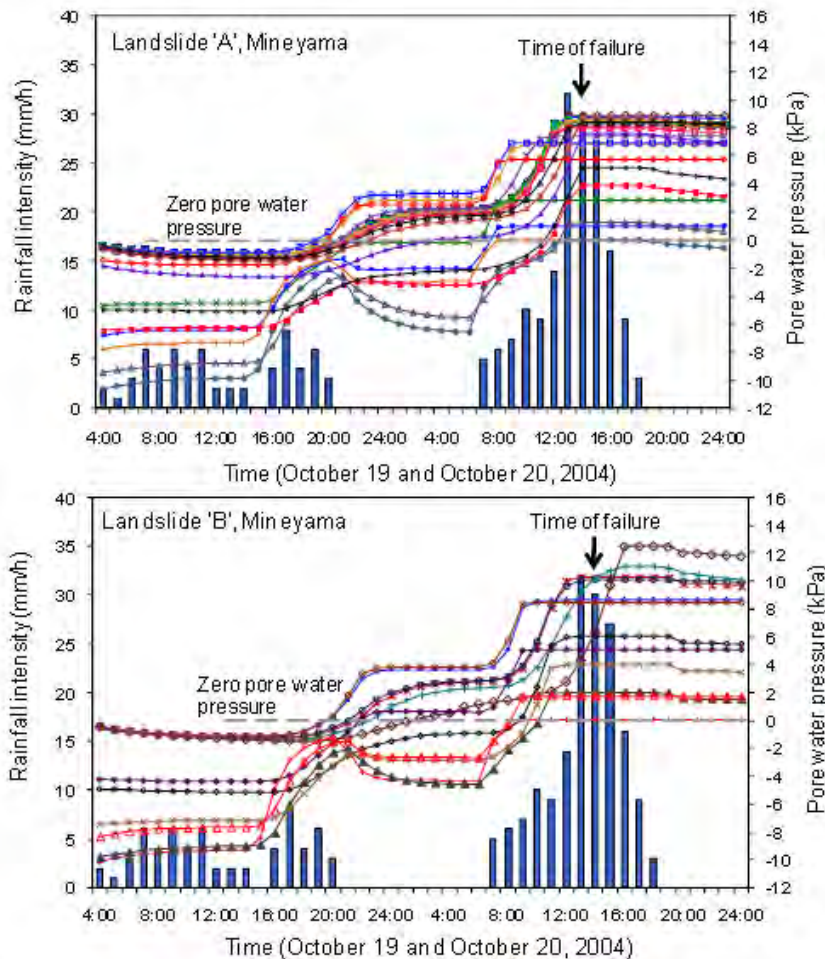
Fig. 11: Schematic illustration of finite element description of slope geometry.

Rate of evaporation was not considered in this modelling and it is an important limitation of this study. In reality, the actual evaporation or evapotranspiration rate from the surface is a function of vegetation cover, soil moisture, and sunlight hour. SEEP/W v.4 of GeoStudio can handle an evaporative flux only by defining a negative flux along the ground surface. Thus, to incorporate evaporation as a negative flux in the seepage analysis, an average evaporation flux rate was applied along the surface during the preliminary phase of analysis. The result of pore pressure reduction, however, was very unrealistic in comparison to the field problems. Other researchers have had similar experiences during seepage analysis (Gasmo et al. 2000; Tsaparas et al., 2002). In general, during extreme typhoon rainfall events negligible evaporation takes place, since this study is focused on the changes in pore water pressures during extreme typhoon rainfall events, evapotranspiration is not a significant Factor Likewise, in the earlier phase of simulation, to ascertain the infiltration process of rain water, a Green-Ampt solution for unsteady rainfall model developed by Parsons and Munoz-Carpena (2000), was used to ascertain the infiltration process at the Mineyama landslides site. Gampt v0.3 follows the method of Chu (1978), Mein and Larson (1973) and Skaggs and Kaheel (1982) to calculate infiltration for unsteady rainfall using the Green and Ampt (1911) equation. Results of Gampt v0.3 suggested that there was no surface ponding period during the rainfall of 19th and 20th October 2004 at the Mineyama landslides site. Thus, surface runoff was not considered in this model and whole rain was assumed to completely infiltrate through soil. Two simulations (for locations A and B) were done. For the simulations, the typhoon rainfall event of 19th and 20th October of 2004 was divided into 2700 time steps of 1 min length (total 45 hours) and seepage into the soil were simulated using SEEP/W v.4 of GeoStudio.

6.1.2 Result of seepage analysis

From the seepage simulation, the values of pore water pressure in both selected slopes were usually high in October 20th 2004, the date of failure. Pore water pressure development was usually transient because of the permeability of soil and potential seepage faces on the slope. Pore water pressure variations in 19th and 20th October of 2004 at the slip surface of both landslides are shown in Fig. 12. The distribution of the water table varies in both simulations. In both simulations, rainfall of 4:00 to 20:00 hours on the 19th October was found to be responsible to saturate soil for several hours. As a result, although there was no rainfall between 20:00 hours of 19th October and 7:00 hours of 20th October, seepage dissipation and continued increment of pore water pressure were observed at many nodes along slip surfaces during that period. Consequently, rainfall between 7:00 hours and 14:00 hours of 20th

522 October increased the pore water pressure to a maximum of 9 kPa in some nodes of
 523 Landslide 'A' and around 12 kPa in some nodes of landslide 'B' (Fig. 12).



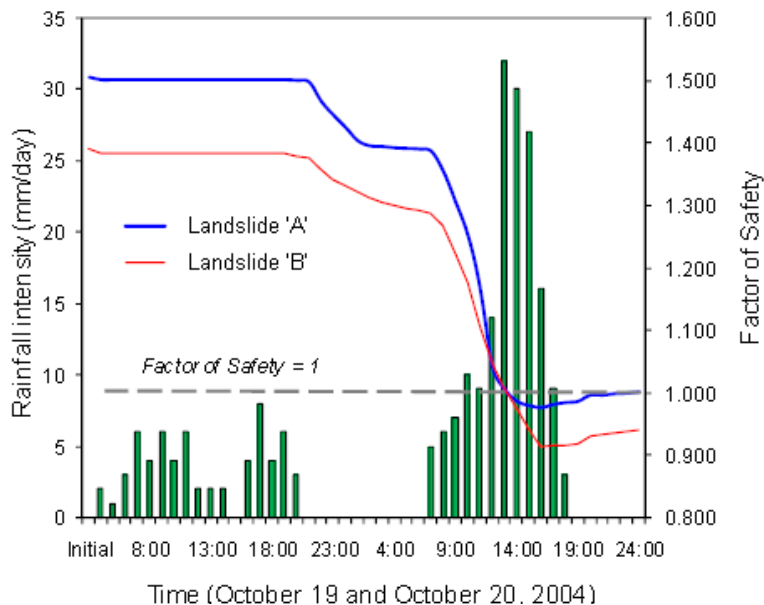
524
 525
 526 **Fig. 12: Pore water pressure variation in 19th and 20th October of 2004 at the slip**
 527 **surface. The location of slip surfaces were fixed as per the field measurement and are**
 528 **shown in Fig 10 for both sites. Curves of low pore water pressure resemble pore water**
 529 **pressure at nodes of higher elevation along the slip surface.**

530 **6.1.3 Stability analysis and result**

531 Slope stability analyses were conducted for both landslide locations, using pore water
 532 pressures determined at different time steps as input data for a limit equilibrium analysis
 533 performed with SLOPE/W v.4 software (GeoStudio 2005). The factor of safety of the soil
 534 cover was computed with the Morgenstern-Price method. In both models, fully specified
 535 (GeoStudio 2005) slip surface (same as failure condition of 20th October 2004) was used at a
 536 surface distance of 25 m from the upslope edge and down slope edge (see Fig. 10). During
 537 the stability analysis, critical slip surfaces were optimized with a maximum of 2000 iterations.
 538 In the simulation, the fully specified slip surface was also optimized to obtain the most
 539 critical value.

540 The average measured value of unit weight, cohesion and friction angle (Table 1) may vary
 541 from the actual values of natural slopes. The measured angle of friction and unit weight are
 542 relatively low probably because of organic content (dead roots) on soil. Therefore sensitivity
 543 analysis was done in the stability analysis. Sensitivity analysis is a heuristic analysis which
 544 examines the dependency of various parameters used in a calculation. Therefore, sensitivity
 545 analysis carries out along with stability analysis to assess the variations in the factor of safety
 546 with respect to changes in engineering parameters such as cohesion, friction angle, and unit

547 weight. Thus, in the present study, the factor of safety distribution via sensitivity calculation
 548 (an option available in Slope/W) was considered to get the factor of safety distribution value.
 549 For this purpose, minimum and maximum values of cohesion, friction angle, and unit weight
 550 measured in the field were used to estimate value of delta and steps from the mean.
 551 In all simulations, factors of safety decreased abruptly from 7:00 hours of 20th October 2004.
 552 At the time of failure (14:00 hours), the factor of safety at landslide 'A' was less than 1.
 553 Similarly, for landslide 'B', although time of failure was not known for this landslide, the
 554 factor of safety was found to be less than 1 after 14:00 hours and it is congruent with the
 555 previously assumed time of failure. The variation of factor of safety in both modelling
 556 scenarios is shown in Fig. 13.



557 Time (October 19 and October 20, 2004)
 558 **Fig. 13: Change of factor of safety with rainfall in 19th and 20th October of 2004. The**
 559 **seepage dissipation and continue increment of pore water pressure after rainfall of 19th**
 560 **October possesses substantial effect in reduction of factor of safety of slope on 20th**
 561 **October**

562 7 Discussions and conclusions

563 In this paper, a comprehensive geological, geomorphological, and geotechnical investigation
 564 is discussed to understand the contributing parameters involved in landsliding triggered by
 565 typhoon rainfall in the andesitic terrain.

566 The X-ray diffraction study confirmed that the soil consists of quartz, feldspar, metahalloysite
 567 and illite as major constituent minerals, along with significant amounts of smectite, and
 568 amorphous silica. Smectite was detected in the soil from X-ray analysis. When such swelling
 569 minerals are present in slope materials, the slopes are prone to failure. Swelling minerals such
 570 as smectites expand when they become wet as water enters the crystal structure and increases
 571 the volume of the mineral. During rainfall, they would swell and slopes become prone to
 572 failure. Previous studies (Kerr 1972; Bardou et al. 2004; Yatabe et al. 2000) involving the
 573 role of swelling clay minerals in activating a landslide have shown that even a small amount
 574 of swelling clay minerals in soil greatly affects its strength behaviour. Thus, the presence of
 575 swelling minerals in the soils of the study area increase the probability of landslides in the
 576 Mineyama hillock.

577 The residual soil above the bedrock mainly consists of silty clay with fine sand and granules.
 578 In situ measurements of permeability of soil revealed that the soil is moderately permeable
 579 and have hydraulic conductivity in the range of 10^{-7} m/s. The residual soil is well vegetated
 580 by shallow rooted vegetation, is relatively loose, and its bulk density is relatively low. Thus,

581 rainwater can easily infiltrate within the soil. The thickness of residual soil on slopes is also
582 supporting the issue of infiltration and failure. On the scar of the Mineyama landslides, the
583 average soil thickness was 1.2 m. This thickness on uphill slopes (average inclination 28° to
584 35°) of zero order basins is found to be favourable for landsliding.

585 After understanding of geological and geomorphological setting of the area as well as
586 geotechnical properties of slope materials, seepage modelling and stability analysis were
587 performed. Hourly rainfall data was used in the simulations. Fluctuation of transient pore
588 water pressure with respect to rainfall was observed in the both simulated slopes. The
589 stability analysis of the simulated slopes showed that the factor of safety was less than 1 after
590 14:00 hours on the 20th October 2004. The reported time of failure by eyewitness account
591 tally with the simulated time. Thus the modelling was significant and representing the real
592 scenario. The transient pore water pressure and factor of safety variations in the andesitic
593 slopes during typhoon rainfall were understood from this modelling. In general, the andesitic
594 slopes are prone to failures due to the significant pore water pressure response to the rainfall,
595 which leads to the considerable loss of soil matric suction and rise of positive pore water
596 pressure under moderately intense rainfall.

597 Similarly, seepage modelling suggested that the water dissipation period of slope materials in
598 andesitic terrain was comparatively large. As a result, pore water pressure was increased at
599 later stage of first phase rainfall (i.e. 19th October, 2004). Presence of more than 50% of fines
600 (silt and clay) in slope materials supports the lower rate of seepage dissipation. When, the soil
601 permeability with respect to water is low (in the range of 10^{-7} m/s) then the pore water
602 pressures may not change significantly during the rainfall, but they can start increasing
603 towards positive values after the end of the wet period (Tsaparas et al., 2002). Same situation
604 was appeared in the case of Mineyama landslides also and there was not any significant
605 change in pore water pressure during first phase of rainfall. During forty-five hours of
606 typhoon rainfall events, there was a period of 10 hours (in night) of no rainfall. Seepage
607 simulation suggested that the first phase rainfall of 19th October, 2004 was depicting
608 antecedent moisture effect on soil. Consequently, when rainfall started at 7:00 hours of 20th
609 October, 2004, the factor of safety of slope decrease abruptly and failure occurred at 14:00
610 hours.

611 The following concluding remarks can be drawn from this study.

- 612 • Soil characteristics, low internal friction angle of fines in soil, and the presence of clay
613 minerals were the main contributing parameters for slope failures on Mineyama hillock.
- 614 • The clay mineralogy of slope materials was also a major contributing factor for rainfall-
615 induced landslides in the andesitic terrain.
- 616 • Results indicate that the simulation of the saturated and unsaturated flow within the soil,
617 using a finite element seepage analysis can provide useful information of the pore water
618 pressure, total head and volumetric water content in response to the different intensity
619 and phases of the typhoon rainfall event.
- 620 • The results of this study show that transient pore water pressure distribution appears to
621 be a key triggering mechanism behind rainfall-induced slope failures in residual soil
622 slopes of andesitic terrain. Other researchers in the residual soils of granitic and
623 sedimentary terrains (Rahardjo et al. 1995; Rahardjo et al. 2002, Rinaldi et al. 2004;
624 Dapporto et al. 2005; Dahal et al. 2008a) make similar observations.
- 625 • Antecedent rainfall affects landslide stability by reducing soil matric suction and
626 increasing transient pore water pressure. Seepage analysis clearly suggests that
627 antecedent moisture content vigorously enhance the pore water pressure build-up the
628 failure process in the residual soil of andesitic terrain in west Japan. Thus, in the
629 andesitic terrain of western Japan, typhoon rainfall of one or two days is always
630 responsible for shallow slope failures.

631 **8 Acknowledgements**

632 The authors would like to thank Ms. Aika Mino, Mr. Toshiaki Nishimura, Mr. Toru Mimura,
633 Mr. Yasushi Hamada and Mr. Toshiaki Takabatake for their help in the collection of field
634 data. The authors also acknowledge local forest office of Takamatsu City for providing
635 permission to enter the forest for investigation. Dr. J. E. Parsons of NC State University and
636 Dr. R. Munoz-Carpena of University of Florida are sincerely acknowledged for providing
637 free access to Gampt (Green-Ampt Infiltration for Unsteady Rainfall Model) software. Mr.
638 Anjan Kumar Dahal is acknowledged for his technical support during the preparation of this
639 paper. Finally, special thanks go to the two anonymous reviewers for their useful comments
640 that improved the manuscript substantially.

641 **9 References**

- 642 Aleotti P., 2004,, A warning system of rainfall-induced shallow failure. *Engineering Geology*
643 v 73, pp 247-265.
- 644 Anderson M.G. and Lloyd D.M., 1991, Using a combined slope hydrology-stability model to
645 develop cut slope design charts, *Proceedings of the Inst. of Civil Engineers*, v 91, pp
646 705-718.
- 647 Anderson S.A. and Sitar N., 1995, Analysis of rainfall-induced debris flows. *ASCE Journal*
648 *of Geotechnical Engineering* v. 121(7), pp 544–552.
- 649 Bardou, E., Bowen, P., Banfill, P. G., Boivin, P., 2004, Dramatical impact of low amounts of
650 swelling clays on the rheology of alpine debris flows, *Eos Trans. AGU*, 85(47), Fall
651 Meet. Suppl., Abstract H41B-0293.
- 652 Beven, K.J., Kirkby M.J., 1979, A physical based variable contributing area model of basin
653 hydrology, *Hydrological sciences Bulletin*, v 24 (1), pp 43-69.
- 654 Borga M., Dalla F.G., Gregoretti C., Marchi L., 2002, Assessment of shallow landsliding by
655 using a physically based model of hillslope stability, *Hydrol. Processes* v 16, pp
656 2833-2851.
- 657 Brand E.W., Permchitt J., Phillison H.B., 1984, Relationship between rainfall and landslides
658 in Hong Kong. *Proceedings of the 4th International Symposium on Landslides*, v 1,
659 pp 377–384.
- 660 Cai F. and Ugai K., 2004, Numerical Analysis of Rainfall Effects on Slope Stability,
661 *International Journal of Geomechanics* v 4, pp 69-78.
- 662 Caine N., 1980, The rainfall intensity-duration control of shallow landslides and debris flows.
663 *Geografiska Annaler* v62A, pp 23–27.
- 664 Campbell R.H., 1975, Soil slips, debris flows, and rainstorms in the Santa Monica Mountains
665 and vicinity, Southern California. U.S. Geological Survey Professional Paper 851, pp
666 1 – 20.
- 667 Chu, S.T., 1978, Infiltration during unsteady rain. *Water Resources Research*. v 14(3), pp
668 461-466.
- 669 Collins B.D. and Znidarcic D., 2004, Stability analyses of rainfall induced landslides. *Journal*
670 *of Geotechnical and Geoenvironment Engineering* v 130, pp 362–372.
- 671 Collison A.J.C. and Anderson M.G., 1996, Using a combined slope hydrology/slope stability
672 model to identify suitable conditions for landslide prevention by vegetation in the
673 humid tropics. *Earth Surface Processes and Landforms* v 21, pp 737-747.
- 674 Corominas J. 2000, Landslides and climate. In: *Proceedings 8th International Symposium on*
675 *Landslides*, Bromhead E., Dixon N., Ibsen M.L., eds., A.A. Balkema, v 4, pp 1–33.
- 676 Crosta G.B. and Dal Negro P., 2003, Observations and modelling of soil slip-debris flow
677 initiation processes in pyroclastic deposits: the Sarno 1998 event, *Natural Hazards and*
678 *Earth System Sciences* 3:53–69.
- 679 Crozier M.J.,1999, Prediction of rainfall-triggered landslides: a test of the antecedent water
680 status model. *Earth Surface Processes and Landforms* v 24, pp 825– 833.

681 Dahal R.K., Hasegawa S., 2008, Representative rainfall thresholds for landslides in the Nepal
682 Himalaya, *Geomorphology*, v 100 (3-4), pp 429-443.

683 Dahal R.K., Hasegawa S., Nonomura A., Yamanaka M., Masuda T., Nishino K., 2008a,
684 Failure characteristics of rainfall-induced shallow landslides in granitic terrains of
685 Shikoku Island of Japan, *Environmental Geology*, online first, DOI: 10.1007/s00254-
686 008-1228-x

687 Dahal R.K., Hasegawa S., Yamanaka M., Nishino K., 2006, Rainfall triggered flow-like
688 landslides: understanding from southern hills of Kathmandu, Nepal and northern
689 Shikoku, Japan. Proc 10th Int Congr of IAEG, The Geological Society of London,
690 IAEG2006 Paper number 819: pp 1-14 (CD-ROM)

691 Dahal R.K., Hasegawa S., Yamanaka M., Nonomura A., 2008b, Typhoon rainfall and
692 landsliding in the Pacific Ocean side of Japan, proceedings of the eighteenth (2008)
693 international offshore and polar engineering conference Vancouver, BC, Canada, pp
694 795-802

695 Dahal R.K., Hasegawa S., Yamanaka M., Dhakal S., Bhandary N.P., Yatabe R., 2009,
696 Comparative analysis of contributing parameters for rainfall-triggered landslides in
697 the Lesser Himalaya of Nepal, *Environmental Geology*, v 58(3), pp 567-586.

698 Dai F., Lee C.F., Wang S.J., 1999, Analysis of rainstorm-induced slide-debris flows on
699 natural terrain of Lantau Island, Hong Kong. *Engineering Geology* v 51, pp 279-290.

700 Daitou Techno Green, 2009, Hasegawa in situ permeability tester, operating manual V.3.1,
701 available for download in <http://www.daitoutg.co.jp/prd/pdf/tousui0703.pdf>

702 Dapporto S., Aleotti P., Casagli N., Polloni G., 2005, Analysis of shallow failures triggered
703 by the 14–16 November 2002 event in the Albaredo valley, Valtellina (Northern
704 Italy), *Advances in Geosciences* v 2, pp 305–308.

705 Dhakal A.S., Sidle R.C., 2004, Distributed simulations of landslides for different rainfall
706 conditions. *Hydrological Processes* v 18, pp 757–776.

707 Ellen S.D., Fleming R.W., 1987, Mobilization of debris flows from soil slips, San Francisco
708 Bay region, California. In, Costa JE, Wieczorek GF eds., *Debris Flows/Avalanches:
709 Process, Recognition, and Mitigation*, Vol. 7. Boulder, CO: Geol. Soc. Am. Rev. Eng.
710 Geol. pp 31–40

711 Fredlund D.G. and Morgenstern N.R. 1976, Constitutive relations for volume change in
712 unsaturated soils. *Canadian Geotechnical Journal* 13: 261-276.

713 Fredlund D.G., Morgenstern N.R., 1977, Stress state variable for unsaturated soils. *ASCE* v
714 103, pp 447-464.

715 Fredlund D.G., Rahardjo H., 1993, *Soil mechanics for unsaturated soils*, John Wiley & Sons,
716 Inc., p 517

717 Gasmo J.M., Rahardjo H., Leong E.C., 2000, Infiltration effects on stability of a residual soil
718 slope. *Computers and Geotechnics* v 26(02), pp 145–65.

719 GeoStudio, 2005, *GeoStudio Tutorials includes student edition lessons*, 1st edition revised,
720 Geo-Slope International Ltd., Calgary, Alberta, Canada.

721 Giannecchini R., 2006, Relationship between rainfall and shallow landslides in the southern
722 Apuan Alps (Italy), *Nat Hazards Earth Syst. Sci.* v 6, pp 357-364.

723 Glade T., Crozier M., Smith P., 2000, Applying probability determination to refine landslide-
724 triggering rainfall thresholds using an empirical Antecedent Daily Rainfall Model,
725 *Pure and Applied Geophysics* v 157, pp 1059–1079.

726 Gray D.H., Leiser A.T., White C.A., 1980, Combined vegetative-structural slope
727 stabilization. *Amer. Assoc. Civil Eng.* v 50(1), pp 82-85.

728 Green W.H. and Ampt G.A. 1911, Studies on soil physics: 1. Flow of air and water through
729 soils. *J Agr Sci* v 4, pp 1–24.

730 Greenway D.R., 1987, Vegetation and slope stability. In: Anderson M.G., Richards K.S.
731 (eds.) Slope stability. Wiley, New York, pp 187–230.

732 Guzzetti F, Cardinali M, Reichenbach P, Cipolla F, Sebastiani C, Galli M, Salvati P. (2004)
733 Landslides triggered by the 23 November 2000 rainfall event in the Imperia Province,
734 Western Liguria, Italy, *Engineering Geology* v 73, pp 229–245.

735 Hayashi S., 1998, The study of the re-vegetation plant stability on the slope considering of
736 the characteristics of wind resistance, Report of grant-aid for the science research in a
737 year of Heisei 7th – 9th, pp 9-21 (in Japanese)

738 Hiura H., Kaibori K., Suemine A., Satofuka Y., Tsutumi D., 2004, Sediment-related disaster
739 in Kisawa Village and Kaminaka Town in Tokushima Prefecture, Japan, induced by
740 the heavy rainfall of the Typhoon Namtheun in 2004 (prompt report), *Journal of the*
741 *Japan Society of Erosion Control Engineering*, v 57(4), pp 39-47 (in Japanese).

742 Howell J., 1999a, Roadside Bio-engineering, HMG Nepal, Department of Roads, Babar
743 Mahal, Kathmandu, Nepal, Reference Manual, p. 216.

744 Howell J., 1999b, Roadside Bio-engineering, HMG Nepal, Department of Roads, Babar
745 Mahal, Kathmandu, Nepal, Site Handbook, p. 160.

746 Iverson R.M., 1997, The physics of debris flows, *Reviews of Geophysics* 5: 245–96.

747 Iverson R.M. 2000, Landslide triggering by rain infiltration, *Water Resources Research*
748 36(7): 1897-1910.

749 Iverson R.M., Reid M.E., La Husen R.G., 1997, Debris-flow mobilization from landslides.
750 *Annual Review of Earth and Planetary Sciences* v 25, pp 85–138.

751 Kerr P.F., 1972., The Influence of Clay Minerals on Surficial Earth Movements, Final rept.,
752 Columbia University New York Dept of Geology, 24 p.

753 Kim J., Jeong S., Park S., Sharma J., 2004, Influence of rainfall-induced wetting on the
754 stability of weathered soils slopes, *Engineering Geology* v 75, pp 251–262.

755 Kondo K., Nonoda T., Hayashi S., Numamoto S., 2004, Analytical study on the role of tree
756 roots system in slope stability, *Journal of Japan Landslide Society* v 41(3), pp 39-47.

757 Krahn J., 2004a, Seepage modeling with SEEP/W, An engineering Methodology, 1st edition,
758 Geo-Slope International Ltd., Calgary, Alberta, Canada.

759 Krahn J., 2004b, Stability modeling with SLOPE/W, An engineering Methodology, 1st
760 edition, Geo-Slope International Ltd., Calgary, Alberta, Canada.

761 Kubota T., Omura H., Okumura T., Tada Y., Paudel P.P., 2004, Influence of the forest tree
762 load on the slope stability with different forest felling, *Journal of the Japan Landslide*
763 *Society* v 41(3), pp 273-281 (in Japanese with English abstract).

764 Kuno H., 1947, Two Orthopyroxenes from the so-called bronzite-andesites of Japan.
765 *Proceedings of the Japan Academy*, v 23(1-11), pp 117-120.

766 Lan H., Zhou C., Lee C.F., Wang S., Wu F., 2003, Rainfall induced landslide stability
767 analysis in response to transient pore pressure - A case study of natural terrain
768 landslide in Hong Kong, *Science in China Ser. E Technological Sciences* 46 supp.:52-
769 68.

770 Mein R.G. and Larson C.L., 1973, Modelling infiltration during a steady rain, *Water Resour.*
771 *Res.* v 9(2), pp 384-394.

772 MLIT, 2004, Information about typhoon disasters of 2004, Shikoku Regional Development
773 Bureau, Ministry of Land, Infrastructure and Transport,” web page
774 <http://www.skr.mlit.go.jp/sabo/dosha/doshaf.html>

775 Montgomery D.R., Dietrich W.E., Torres R., Anderson S.P., Heffner J.T., Loague K., 1997,
776 Hydrologic response of a steep, unchanneled valley to natural and applied rainfall
777 *Water Resources Research*, v 33(1), pp 91–109.

778 Morgan R.P.C. and Rickson R.J., 1995, Slope stabilization and erosion control. E and FN
779 Spon: London, 274p.

780 Nghiem Q.M., Nakamura H., Shiraki K., 2004, Slope stability of forested slopes considering
781 effect of tree root and steel bar reinforcement, *Journal of Japan Landslide Society* v
782 41(3), pp 48-56.

783 Olivares L. and Picarelli L., 2003, Shallow flowslides triggered by intense rainfalls on natural
784 slopes covered by loose unsaturated pyroclastic soils, *Géotechnique* 53(2):283-287.

785 Parsons J.E. and Muñoz-Carpena R., 2000, Gampt v0.3, Green-Ampt Infiltration for
786 Unsteady Rainfall Model, available for download in
787 <http://carpena.ifas.ufl.edu/software/gampt.html> (accessed on 2008-01-25)

788 Rahardjo H., Lee T.T., Leong E.C., Rezaur R.B., 2005, Response of residual soil slope to
789 rainfall, *Canadian Geotechnical Journal* v42(2), pp 340–351.

790 Rahardjo H., Leong E.C., Rezaur R.B., 2002, Studies of rainfall-induced slope failures. In:
791 Paulus P, Rahardjo H (eds) *Slope 2002. Proceedings of the National Seminar, Slope*
792 *2002. 27-April 2002. Bandung, Indonesia*, pp 15–29.

793 Rahardjo H., Lim T.T., Chang M.F., Fredlund D.G., 1995, Shear strength characteristics of a
794 residual soil. *Canadian Geotechnical Journal* v 32, pp 60–77.

795 Reid M.E., Nielson H.P., Dreiss S.J., 1988, Hydrologic factors triggering a shallow hillslope
796 failure, *Bull. Assoc. Eng. Geol.*, v 25, pp 349–361.

797 Rezaur R.B., Rahardjo H., Leong E.C. 2002, Spatial and temporal variability of pore-water
798 pressures in residual soil slopes in a tropical climate. *Earth Surface Processes and*
799 *Landforms*, v 27(3), pp 317–338.

800 Richards L.A., 1931, Capillary conduction of liquids through porous mediums. *Physics* 1:
801 318–333.

802 Rinaldi M., Casagli N., 1999, Stability of streambanks formed in partially saturated soils and
803 effects of negative pore water pressures: the Sieve River (Italy). *Geomorphology*
804 26:253–277.

805 Rinaldi M., Casagli N., Dapporto S., Gargini A., 2004, Monitoring and modelling of pore
806 water pressure changes and riverbank stability during flow events. *Earth Surf*
807 *ProcessLandforms* v 29, pp 237–254.

808 Sassa K., 1998, Recent urban landslide disasters in Japan and their mechanisms. In:
809 *Proceedings of 2nd International Conference on Environmental Management,*
810 *“Environmental Management”*, Australia, 10– 13 February, vol. 1. Elsevier,
811 Amsterdam, pp 47–58

812 Schmidt K.M., Roering J.J., Stock J.D., Dietrich W.E., Montgomery D.R., Schaub T., 2001,
813 The variability of root cohesion as an influence on shallow landslide susceptibility in
814 the Oregon Coast Range, *Can. Geotech. J.* v 38, pp 995–1024.

815 Sidle R.C., 1991, A conceptual model of changes in root cohesion in response to vegetation
816 management, *Journal of Environmental Quality*, v 20(1), pp 43-52.

817 Skaggs, R.W., Khaheel R., 1982, Infiltration, In: *Hydrologic modeling of small watersheds,*
818 *Haan CT, Johnson HP and Brakensiek DL (eds.), St. Joseph, MI, ASAE*, pp 121-168

819 Terlien, M.T.J., 1996, Modelling spatial and temporal variations in rainfall-triggered
820 landslides, PhD thesis, ITC Publ. Nr. 32, Enschede, The Netherlands, 254p.

821 Tofani V., Dapporto S., Vannocci P., Casagli N., 2006, Infiltration, seepage and slope
822 instability mechanisms during the 20–21 November 2000 rainstorm in Tuscany,
823 central Italy *Nat. Hazards Earth Syst. Sci.* 6:1025–1033

824 Tsaparas I., Rahardjo H., Toll D.G., Leong E.C., 2002, Controlling parameters for rainfall-
825 induced landslides, *Computers and Geotechnics* v 29, pp 1–27.

826 Van Genuchten M.T., 1980, A closed-form equation for predicting the hydraulic conductivity
827 of unsaturated soils. *Soil Sc Soc Am J* v 48, pp 703-708.

828 Waldron L.J., 1977, The shear resistance of root-permeated homogeneous and stratified soil,
829 *Soil science society of America Journal*, v 41, pp 843-849.

- 830 Wieczorek G.F., 1996, Landslide triggering mechanisms, in: Landslides Investigation and
831 Mitigation, edited by: Turner AK, Schuster RL, special report 247, National Academy
832 Press, Washington D.C., pp 76–90.
- 833 Wieczorek, G.F. 1987, Effect of rainfall intensity and duration on debris flows in central
834 Santa Cruz Mountains, California, In Debris flows/Avalanches: process, recognition
835 and mitigation, (Eds) Costa J E, Wieczorek GF, Geological Society of America,
836 Reviews in Engineering Geology v 7, pp 93–104.
- 837 Wilson R.C., Wieczorek G.F., 1995, Rainfall threshold for the initiation of debris flow at La
838 Honda, California, Environmental and Engineering Geoscience v 1(1), 11-27.
- 839 Wu T.H., Mckinnell III W.P., Swanston D.N., 1979, Strength of tree roots and landslides on
840 Price of Wales Island, Alaska, Journal of Canadian Geotechnique, v 16, pp 19-33.
- 841 Yatabe R., Yagi N., Yokota K., Bhandary N.P., 2000, Influence of expansive chlorite on the
842 strength of weathered Green Rock at Mikabu Belt of Japan, Proc. International
843 Conference on Geotechnical and Geological Engineering, Melbourne, Australia, Nov.
844 19-24, 2000 (CD format).